

*Fiscal Year 2010
Summary Report on the
Epsilon-Metal Phase as a
Waste Form for ⁹⁹Tc*

Fuel Cycle Research & Development

Prepared for
U.S. Department of Energy
Waste Form Campaign
D. M. Strachan, J. V. Crum, E. C. Buck,
B.J. Riley, and M. R. Zumhoff
Pacific Northwest National
Laboratories
September 2010
FCRD-WAST-2010-000188
PNNL-19828



DISCLAIMER

This information was prepared as an account of work sponsored by an agency of the U.S. Government. Neither the U.S. Government nor any agency thereof, nor any of their employees, makes any warranty, expressed or implied, or assumes any legal liability or responsibility for the accuracy, completeness, or usefulness, of any information, apparatus, product, or process disclosed, or represents that its use would not infringe privately owned rights. References herein to any specific commercial product, process, or service by trade name, trade mark, manufacturer, or otherwise, does not necessarily constitute or imply its endorsement, recommendation, or favoring by the U.S. Government or any agency thereof. The views and opinions of authors expressed herein do not necessarily state or reflect those of the U.S. Government or any agency thereof.

SUMMARY

Epsilon metal (ϵ -metal), sometimes called the five-metal-phase, is generated in nuclear fuel during irradiation (Kleykamp 1985; Kleykamp 1987; Kleykamp 1988; Kleykamp et al. 1985; Kleykamp and Pejsa 1984). This metal consists of Pd, Ru, Rh, Mo, and some Te. These accumulate at the UO₂ grain boundaries as small (ca 5 μ m) particles. This metal has limited solubility in the nitric acid used to dissolve nuclear fuel for recycling with roughly half of the Ru in solution and half left as part of undissolved solids (UDS). The fraction left as UDS is separated from solution by clarification of the dissolver solution and routed for further treatment. Some recycling plants, e.g. La Hague in France and Rokkasho in Japan, send the UDS to the vitrification process. However, ϵ -metal is generally not soluble in typical borosilicate waste glasses. Therefore, the total concentration of UDS is likely to limit the loading of commercial high-level wastes in glass. This is less of a concern for La Hague and Rokkasho because most of the nuclear fuel processed in these plants has not cooled for many years prior to recycling; whereby the waste loading in glass is heat limited. To optimize loading of waste in glass, the ϵ -metal must be treated separately.

There are two reasons for selecting the ϵ -metal phase for use as a waste form. It is found in the UDS from the dissolution of nuclear fuel in strong acid. Remnants of this phase are found in the natural reactors at Gabon, Africa where the environmental conditions were very harsh – much more so than would be expected in a repository, except under the conditions of magma intrusion. The metal waste form would be formed by arc melting the ϵ -metal particles into an ingot without any dilution from other metals.

In the proposed process, the UDS would be combined with soluble Tc (converted to a metal) and, potentially, the other metals removed from the acid stream. The waste form would be formed by arc melting this combined stream into an ingot without any dilution from other metals.

Results to date indicate that the combination of Mo, Pd, Re (Tc), Rh, and Ru yields a metal with nearly invariant unit cell parameters with composition. The metal samples made to date consist of a single phase, but one in which there are high Re and high Pd regions. The X-ray diffraction (XRD) pattern can only be indexed to a single phase with a hexagonal close packing structure and space group P6₃/mmc. These results are similar to those found by Kleykamp and coworkers (1985) for the metal phases with the hexagonal structure found in irradiated fuel.

We also melted metal with 10 mass% ZrO₂ as a stand-in for the other phases present in the UDS. These results indicate that the ZrO₂ was unreacted and remained in the metal as isolated pockets as the mineral baddeleyite. No evidence was found for Zr dissolved into the metal phase. A cubic phase was found that was consistent with the high-temperature XRD results that indicate the ingrowth of a cubic phase above 1000°C. The presence of the cubic phase in this melt is probably the result of the higher temperatures required to melt this material and the rapid quenching of the sample.

The results of the studies done to date suggest that the ϵ -metal is a robust waste form that is flexible with respect to composition. Melting of the metal can be done with a non-volatile oxide, such as ZrO₂, as a stand-in for the oxide portion of UDS. This oxide is immobilized in the metal matrix as isolated pockets. Studies of the UDS have not resulted yet in a clear definition of its composition. Additional studies are needed with more realistic UDS materials.

CONTENTS

<u>SUMMARY</u>	iii
<u>ABBREVIATIONS</u>	ix
<u>1. INTRODUCTION</u>	1
<u>2. Production Methods</u>	2
<u>2.1 Introduction</u>	2
<u>2.2 Waste Composition and Quantity</u>	2
<u>2.3 Arc Melting</u>	2
<u>2.3.1 Advantages</u>	3
<u>2.3.2 Disadvantages</u>	3
<u>2.3.3 Size</u>	4
<u>2.4 Induction Melting</u>	4
<u>2.4.1 Advantages</u>	4
<u>2.4.2 Disadvantages</u>	4
<u>2.4.3 Size</u>	4
<u>2.5 Furnace Melting</u>	4
<u>2.5.1 Advantages</u>	4
<u>2.5.2 Disadvantages</u>	4
<u>2.5.3 Size</u>	5
<u>2.6 Hot Uniaxial Pressing</u>	5
<u>2.6.1 Advantages</u>	5
<u>2.6.2 Disadvantages</u>	5
<u>2.6.3 Size</u>	5
<u>2.7 Hot Isostatic Pressing</u>	5
<u>2.7.1 Advantages</u>	5
<u>2.7.2 Disadvantages</u>	6
<u>2.7.3 Size</u>	6
<u>2.8 Preferred Technology</u>	6
<u>3. Experimental Methods and Materials</u>	6
<u>4. Results</u>	8
<u>4.1 Metal Analyses</u>	8
<u>4.2 X-Ray Diffraction</u>	8
<u>4.3 SEM Characterization</u>	10
<u>4.4 TEM Characterization</u>	11
<u>5. Conclusions</u>	14
<u>6. Future Work</u>	14
<u>7. References</u>	15

FIGURES

Figure 1. Set of XRD patterns from three ϵ-metal alloy specimens. Preferred orientation is evident from the intensity of the diffraction peak at approximately $82^\circ 2\theta$.	8
Figure 2. A summary of XRD patterns showing the effect of increasing temperature on the crystal structure of an ϵ-metal specimen with the base composition. The set of patterns on the left show more clearly the ingrowth of the cubic phase (Im3m); ingrowth is very subtle, occurring as a broadening of the peak on the high angle side. For clarity, the diffraction angles increase in opposite directions in these graphs.	9
Figure 3. A graph showing the variation in lattice parameters with temperature for both the hexagonal and cubic phases. Part of the offset in data sets is from a lack of temperature calibration for the hot stage.	9
Figure 4. A comparison of the positions of two diffraction peaks from the metal phase heated to 1550°C and quenched. The lone diffraction peak at approximately $74^\circ 2\theta$ allowed us to determine the presence of a cubic phase; it could not be established from the high intensity peak at approximately $40.7^\circ 2\theta$.	10
Figure 5. A graph showing the variation in the amount of cubic phase with increasing time at 1550°C.	10
Figure 6. A backscattered electron photomicrograph of the typical microstructure in the ϵ-metal, in this case the base composition plus 25 mass% Re.	11
Figure 7. Electron diffraction pattern taken along the B[121] zone axis, with computer simulation of the diffraction pattern and a molecular model generated from the structural data for hexagonal ruthenium metal.	12
Figure 8. Images showing grown-in defects in metal taken along (a) $g = 002$ and (b) $g = 100$.	12
Figure 9. Convergent beam electron diffraction patterns taken with $g=110$ between compositionally different areas. The yellow box outlines a region that is common to both patterns. Also shown are the results of the EDS analyses of the regions of interest. The insert shows the slight difference in composition.	13
Figure 10. A CBED pattern close to B[121] with some higher order Laue zones indexed.	13

TABLES

Table 1. The quantities of UDS and ϵ-metal per MTIHM for two fuel burn-ups.	3
Table 2. Target base composition for the ϵ-metal.	8
Table 3. Lattice parameters and unit cell volume changes with changes in Re content.	10
Table 4. The typical compositions of the two phases found in the ϵ-metal, where the element in the second column indicates the enriched metal.	11

ABBREVIATIONS

CBED	convergent beam electron diffraction
HIP	hot isostatic pressing
HOLZ	higher order Laue zone
HUP	hot uniaxial pressing
MTIHM	metric tons irradiated heavy metal
MWd/t	Megawatt-days per tonne (metric ton)
PDF	powder diffraction file
SAED	selected area electron diffraction
TEM	transmission electron microscope
UDS	undissolved solids
XRD	X-ray diffraction

WASTE MANAGEMENT CAMPAIGN

1. INTRODUCTION

Epsilon metal (ϵ -metal) is generated in nuclear fuel during irradiation (Kleykamp 1985; Kleykamp 1987; Kleykamp 1988; Kleykamp et al. 1985; Kleykamp and Pejsa 1984). This metal, also known as the five-metal-phase, consists of Mo, Pd, Ru, Rh, Tc, and some Te. These accumulate at the UO₂ grain boundaries as small (ca 5 μ m) particles. During fuel dissolution in nitric acid, these metal particles only partially dissolve and become a major part of the undissolved solids (UDS). These metals have limited solubility in typical borosilicate glass melts and, if they accumulate in the melter bottom, can cause processing difficulties. At the recycling facilities in La Hague in France and Rokkasho in Japan the UDS are clarified from the dissolver solution and combined with high-level waste in the borosilicate glass. As these glasses are generally heat limited, this has a minimal impact on waste loading. In the U.S., however, fuel will be cooled for many years prior to recycling. The UDS can then be treated separately to improve overall waste loading in glass, if glass is the waste form for the bulk of the high-level wastes from used fuel recycling.

Under the current plan (Gombert II 2007), the ϵ -metal is to be heated with Fe or stainless steel (Fe-Cr-Ni) to form an alloy waste form. As an alternate technology, the ϵ -metal could be melted to form ingots that can be disposed without further treatment. The argument for this latter approach is that these metals survive the rather harsh conditions of the fuel dissolver and, hence, must have some modicum of durability. Additionally, there is a natural analogue for this metal that indicates, by inference, that the ϵ -metal has long-term durability.

In Gabon, Africa, there exist several natural reactors that operated approximately 2 Ga ago (Gauthier-Lafaye, Holliger and Blanc 1996; Hidaka and Holliger 1998). These reactors were 'discovered' when U-ore was found to be depleted in ²³⁵U relative to other sources and expected values of this isotope. Subsequent characterization of these ore bodies gave rise to the estimated history of these reactors. It is estimated that these reactors operated for approximately 500 000 y. Conditions in the reactor zone reached 400°C and 30 MPa. As in a present-day commercial reactor, the ϵ -metal was formed. Results from relatively recent studies indicate that these metal particles were formed and contained the same metals as those found in the ϵ -metal phase in U-based fuel from commercial reactors. Results indicate that the 90% of the Pd, Ru, Rh, and Te remained with the ϵ -metal particles; some of the Tc and Mo migrated, but only to the extent of 1 to 10 mm (Utsunomiya and Ewing 2006). Thus, the two long-lived isotopes^a, ⁹⁹Tc ($t_{1/2} = 2.13 \times 10^5$ y) and ¹⁰⁷Pd ($t_{1/2} = 6.5 \times 10^6$ y) were isolated over a significant geologic period. Both active isotopes have long since decayed to non detectable levels, but the fate of ⁹⁹Tc was determined from the enriched levels of stable ⁹⁹Ru, which is the decay product of ⁹⁹Tc; ¹⁰⁷Pd decays to ¹⁰⁷Ag. In the case of Tc, only radioactive elements are produced during fission; some stable Pd is produced.

These two pieces of information about the ϵ -metal led us to propose that consolidation of the UDS, soluble Tc and soluble Pd, Ru, and Rh into an ingot of ϵ -metal without any dilution might be a viable waste form. Without dilution, the number of unit operations to generate a waste form is reduced and the

^a Tellurium also has long-lived isotopes, but they are considered stable for the purposes of performance assessment. These are ¹²³Te and ¹³⁰Te with 1.3×10^{13} and 2.5×10^{21} y, respectively.

equipment requirements simplified. The results from the examination of material from the natural reactors in Gabon, Africa, suggest a high probability that a waste form composed of these metals could survive for the geologic time needed to isolate both ^{99}Tc and ^{107}Pd . Additionally, Cui and coworkers (2001) found dissolution rates that are many orders of magnitude lower than the typical borosilicate glass.

In this document, we report on work carried out during FY 2010 to develop consolidated ϵ -metal as a viable waste form.

We first discuss some of the process options and propose a method for producing the ϵ -metal ingots in a recycling plant. We then discuss the results from the characterization of several metal samples that were produced during FY 2010.

2. Production Methods

2.1 Introduction

After the dissolution of nuclear fuel, UDS remain in the dissolver and are separated. This material consists of the metal alloy that is formed during the irradiation of UO_2 and some other insoluble material, such as ZrO_2 , $\text{ZrMo}_2\text{O}_7(\text{OH})_2 \cdot 2\text{H}_2\text{O}$, and ZrMo_2O_8 . There is likely to be some other undissolved material as well, but those have not been included in this study. The amounts of ϵ -metal and UDS are relatively small, amounting to at most about 30 kg of waste per day assuming an 800 metric tons of irradiated heavy metal (MTIHM) per year plant. Although the actual density of the ϵ -metal phase is not well known, some of the constituent metals have densities of $12 \times 10^4 \text{ kg/m}^3$. At this density, the maximum volume of metal produced would be about 2.5 L/d. The density calculated from the constituent pure metal densities is $11.7 \times 10^4 \text{ kg/m}^3$. Adding Tc and noble metals from the soluble inventory would increase the volume to about 3 L/d.

There are a number of technologies that could be used to produce this small quantity of metal. They include arc melting, induction melting (inert gas or vacuum), hot uniaxial pressing (HUP), and hot isostatic pressing (HIP). These are discussed below with both the advantages and disadvantages of each. There are some characteristics of the waste that may cause some of these technologies to be less adaptable than others. For example, the Tc vapor pressure might be high enough during arc melting to cause serious losses.

2.2 Waste Composition and Quantity

Table 1 shows the forecast composition of the waste both as UDS and as ϵ -metal phase alone. There is a small contribution to the waste from Zr, presumably as undissolved Zircaloy from the cladding or ZrO_2 as a Zircaloy corrosion product. As indicated, there is likely to be other UDS, but these are as yet unknown. It is important to recognize this when selecting a process to convert these into a solid; the process should be flexible to the waste composition.

2.3 Arc Melting

In this method, a high frequency arc is used to generate a plasma to melt the target material. There are basically two methods by which this can be done. First, a pressed pellet of the metal to be melted is placed on a water-cooled hearth and the arc is struck between a tungsten rod and a grounded metal spike. The arc is then moved to the pellet by moving the tungsten wand, usually by hand. Temperatures in excess of 3000 K are achieved, although this can be varied by controlling the power input. The wand is moved back and forth to achieve good stirring of the molten mass and even melting. In the second method, a crucible containing an initial charge of ϵ -metal is the place where the initial melting takes place. Additional metal is added after the initial charge is molten. More charges of metal, whether in the form of ϵ -metal or ^{99}Tc and platinum group metals from other parts of the process, are added to form a

Table 1. The quantities of UDS and ϵ -metal per MTIHM for two fuel burn-ups.

100 MWd/t	Element (UDS)	g/MTIHM	Epsilon Metal
	Zr	550	
	Mo	2027	2027
	Tc	1011	1011
	Ru	3110	3110
	Rh	346	346
	Pd	4514	4514
Sum		11558	11008
Plant production, MTIHM/y	800		
Production, kg UDS/y		9247	8806
Production, kg/d		30	28
Production efficiency	0.85		

25 MWd/t	Element (UDS)	g/MTIHM	Epsilon Metal
	Zr	134	
	Mo	507	507
	Tc	309	309
	Ru	746	746
	Rh	155	155
	Pd	1035	1035
Sum		2884	2751
Plant production, MTIHM/y	800		
Production, kg UDS/y		2307	2200
Production, kg/d		7	7
Production efficiency	0.85		

single billet of metal that can then be disposed. In the arc melting process, a gas atmosphere is required to carry the arc. Typically, an inert gas, such as Ar or 3 vol% H₂ in Ar either static or flowing, is used. Contaminating gases, typically O₂, are first removed by melting a small sample of Ti or W metal. This is not possible in a flowing gas configuration.

2.3.1 Advantages

This method is very fast. The arc melting process takes place in seconds to minutes. The metal is cooled rapidly because the melting is done on a water-cooled hearth. This also prevents the melt from sticking to the hearth.

2.3.2 Disadvantages

Because this method requires gas to be present albeit inert gas, some contamination is likely. However, the main disadvantage is the likelihood of high volatility of one or more of the metals. This generates problems for cleanup (the inside of the arc melter) to minimized radiation to the workers and off-gas cleanup (secondary waste or recycle). Although the process as envisioned incorporates any non-metallic materials into the metal as isolated pockets, accumulation of slag may cause problems with arc melting. The slag will need to be disposed as secondary waste or accumulated to be disposed along with the rest of the metal.

2.3.3 Size

The part of the unit that needs to be isolated – in radioactive space – is relatively small. Laboratory arc melters occupy approximately 1 m^3 volume with a foot print of approximately 1 m^2 . An arc melter with the capacity to handle approximately 3 L of metal per day would occupy about twice that of the laboratory melter or the equivalent of a cube 1.25 m on a side. The power supply can be outside the radioactive space and has a relatively small foot print similar to a small welding unit.

2.4 Induction Melting

In induction melting, a crucible is heated either through a susceptor or directly with a radio frequency induction coil; the metal itself absorbs the radio frequency energy. The unit can be flushed with inert gas or run under vacuum. In the case of flowing gas, the system can be configured to run continuously and the liquid poured into a canister.

2.4.1 Advantages

These units are commercially available. They are easy to run. The metal is heated quite rapidly- in minutes to perhaps 10 minutes. The cycle time is short allowing for multiple runs to be made during the day, hence a smaller melter.

2.4.2 Disadvantages

As with the arc melter, volatility is the major disadvantage. Slag accumulation also represents a disadvantage, because the slag may need to be disposed as secondary waste.

2.4.3 Size

These melters occupy approximately 8 m^3 with a footprint of about 4 m^2 . The power unit is located outside of the radioactive space. They are typically the size of a file cabinet.

2.5 Furnace Melting

This method could be set up as a continuous or batch operation. Because of the high temperatures involved and the reactivity of the constituent metals to O_2 in air, these operations would have to take place in an inert atmosphere. Since the molten metal is reactive with typical crucible materials, such as alumina or graphite, a graphite crucible with a coating of CeO_2 or ZrO_2 would have to be used. The metal powders would be added either continuously or in batch to the crucible. In continuous operation, the overflow from the crucible would go to a cold canister that would be located in an airlock from which the crucible could be removed and a new one put in its place. An alternate batch operation would be to place crucibles filled with metal powder on a conveyor through a tunnel furnace with the correct temperature profile and inert gas atmosphere. These high temperature furnaces are commonly used in the preparation of nuclear fuel pellets and operate at about 1500°C with a H_2 atmosphere in a glove box.

2.5.1 Advantages

Since there is a large body of experience with these types of furnaces, safe and efficient operations can be assured. Near continuous operation can be achieved. The sizing of the furnace would be scaled to meet the low demand of this operation.

2.5.2 Disadvantages

The footprint for these furnaces is the largest of those discussed to this point. Coated crucible lifetime could be a problem especially if they are single use. Single use would mean that there would be significant secondary waste volume. If a H_2 atmosphere is needed, implementation of extra safety measures and off-gas handling will be needed. While the footprint of a single batch furnace would be smaller than a tunnel furnace, the operation of the furnace would be complicated by the use of high

temperatures in a confined space and the batch operation. The possibility of single-use crucibles is also present.

2.5.3 Size

As mentioned above, the footprint can vary quite a bit depending on the furnace type. This can be on the order of 1 m² to 10s of square metres.

2.6 Hot Uniaxial Pressing

With hot uniaxial pressing, the metal powders are loaded into a die, usually graphite (perhaps coated) or alumina, and an opposing punch inserted from above. The die and punch assembly is heated to some temperature at which the powders consolidate. Again because the metals react with O₂, the operation would have to be carried out in an inert atmosphere or under vacuum. The temperature used in this method would not be high enough to cause the metal or any alloy to melt, but sufficiently high to allow sintering of the metal to near theoretical density. One physical phenomenon that needs to be addressed is the volume changes that might occur as a various crystal phases form during the cooling of the metal. Slight expansions can cause the die body to be destroyed. However, this would be determined before a process was installed in an operating plant.

2.6.1 Advantages

This process would be an inherently lower temperature process than those discussed above. Volatility of the metal with the highest vapor pressure would be essentially eliminated, since the temperatures are low and the system is 'sealed' during the consolidation step. Any oxides would be encapsulated into the metal waste form.

2.6.2 Disadvantages

Unless there is a method of performing the loading of the die while it is hot, this process is inherently a slow process. Thus, the die and punch set needs to be cooled after the consolidation has been achieved. Although large die and punch sets are available, it is uncertain if large enough ones (~2 L maximum for 100 MTIHM fuel case; 0.5 L for 25 MTIHM [Table 1]) are available to match the daily throughput requirements with a one cycle per day process. Additionally, these presses occupy a lot of space; the larger the die and punch set, the larger the occupied space.

2.6.3 Size

The footprint is likely to be on the order of 8 m² and the height up to 3 m.

2.7 Hot Isostatic Pressing

Hot isostatic pressing is a variant of hot uniaxial pressing – consolidation under external gas pressure and temperature. In this case, the metal powder is loaded into a metal can, perhaps coated with a CeO₂ or ZrO₂. The can is evacuated and placed in a pressure vessel that contains heating elements. The temperature of the can is raised on some predetermined schedule while pressure is applied through gas pressure inside of the heated pressure vessel. Since the gas pressure is uniform (isostatic), the can and contained waste consolidates in all directions. The cans are designed in such a way as to facilitate the consolidation and yield a product with roughly uniform dimensions that is easily handled. The temperatures that are needed are insufficient to cause any melting in the product can. Volume changes from phase changes on cooling should not affect the integrity of the main containment.

2.7.1 Advantages

This process would inherently be a lower temperature process than arc, furnace, or induction melting. Volatility of the high vapor pressure metals would be eliminated because of the lower temperature and the sealed can. Hot isostatic pressing in radioactive waste management has been avoided for many years.

However, it continues to be promoted by the scientists at the Australian Nuclear Science and Technology Organization and is now the baseline process for one of the wastes at the Idaho National Engineering Laboratory site.

2.7.2 Disadvantages

This apparatus occupies a large space for the pressure vessel, controls, and gas handling and storage. Because it is a high pressure device, the safety requirements are likely to increase the footprint over that in a typical non-nuclear installation. The containment cans need to be carefully designed. A very reliable apparatus to seal the cans is needed to avoid a leak and possible subsequent contamination of the pressure vessel. The temperature of the process must remain below the softening point of the can material which may require very long time at temperature and pressure to consolidate the ϵ -metal. The large thermal mass of the HIP unit requires slow heating and cooling relative to other options.

2.7.3 Size

A typical unit in which about 3 L of metal could be processed at once is about 2 m \times 1 m for the control unit plus about 2 m \times 2.5 m for the pressure vessel and associated equipment.

2.8 Preferred Technology

It is too early in the development process to down select between the fabrication methods. However, arc melting seems to be a good process for making the ϵ -metal waste form for testing and has been used by many other researchers. The speed with which the product can be made and the flexibility of the process are the determining factors. Although the throughput does not need to be great, the speed with which the metal can be heated and cooled should minimize the volatile losses. The process can be made semi-continuous resulting in a single 3 L or three 1 L cans per day, depending on the burn-up of the fuel being processed. It is also a technology readily adapted to remote or glove box operation. Remote operation may be needed, since the ϵ -metal residual in the fuel dissolver could contain enough trace radionuclides that the radiation field might require remote operation.

3. Experimental Methods and Materials

Consistent with the production method assessment and, for very practical reasons, availability of equipment in which these metal alloys could be made, we arc-melted the samples described below. In the initial studies reported here only non-radioactive metals were used in testing with Re substituted for Tc. Four of the metals (Mo, Re, Ru, and Rh) were purchased from Alfa Aesar (Ward Hill, MA) as approximately 325-mesh and 99.999% purity powders; Pd was from an existing stock of much coarser powder, but of equal purity.

Previous studies (Wronkiewicz et al. 2002) indicated that a two pellet procedure was advisable. This was because the melting point of Re (3180°C) exceeds the boiling point of Pd (2940°C). Therefore, a pellet containing Re and Mo were combined by thoroughly mixing the metal powders with a small amount of polyvinyl alcohol (PVA) binder; pressing a pellet at 21 MPa in a small laboratory press; isostatically pressing at 0.45 GPa; and slowly heating the pellet under N₂ to 200°C for 4 h then to 600°C for 0.5 h to burn out the binder. Similarly, a pellet containing the Pd, Ru, and Rh was made. These pellets were separately melted in a laboratory arc melter under flowing Ar/3.75% H₂ on a water-cooled Cu hearth. The two resulting pellets were placed one on top of the other and arc melted. This technique was only necessary because the metals were not already combined in an ϵ -metal phase and because Re was used as a stand-in element. During implementation, the arc melting technique would be much simplified as described in Section 2.3.

Subsequent to the first pellet being made with the above process, we investigated the possibility of combining the metals together in the desired ratios and making a single pellet that was arc melted. This

method resulted in a pellet with similar characteristics to the sample made with the two-pellet method. With this success, we abandoned the two pellet method.

We also sampled the off-gas from the arc melter to determine if significant metal loss was evident. Subsequent analyses showed that no metal was lost to the off-gas from the arc melter. However, the mass loss needs to be verified by measuring the mass before and after the arc melting that needs to be done at a number of power settings, as the Pd or other metals may plate out on virtually any cold surface.

To simulate addition of Tc from recycle of the soluble Tc, we added an additional 25, 50, and 100 mass% extra Re to individual samples. These alloys became increasingly harder to melt with increasing Re content; all were successfully melted. Again, the melting temperature of Re (3180°C) is significantly higher than that of Tc (2170°C).

To simulate the case where UDS is melted, we made a sample in which we added 10 mass% ZrO₂ powder. The samples were prepared in the same manner as described above for the pure metal samples.

Specimens were characterized with scanning electron microscopy (SEM; JEOL JSM-5900, Tokyo, Japan) with secondary electron and backscatter electron imaging. Energy dispersive spectroscopy (EDS) was performed with an energy-dispersive X-ray spectroscopy (EDAX) Li-drifted Si detector. X-ray diffraction (XRD; Bruker D8 advanced diffractometer with parallel beam, Madison, WI). The XRD had a high temperature attachment with an AlN specimen support (Anton Parr HTK 16, Ashland, VA). The hot stage has a graphite heating strip on which the AlN composite sample holder rests. Transmission electron microscopy (TEM; Tecnai T30, FEI Inc., Hillsboro, OR) with EDS analyses performed with a light element EDAX detector with embedded Tecnai analysis software (Emispec Corp. [part of FEI]) and an Orius digital camera (Gatan, Inc., Pleasanton, CA). Thin specimens for the TEM were obtained by first polishing to a very thin specimen, then ion-milling to a TEM-suitable thickness.

To reduce preferred orientation in the XRD, some specimens were prepared by first cooling them in liquid nitrogen followed by crushing in a hardened steel die and hammer. The cooling and crushing procedure was repeated until enough fine powder was available to fill either a glass capillary (room temperature scans) or to produce a thin powder layer covering the AlN holder (high temperature scans). Crystalline phases were identified with Jade 6.0 software and both the ICDD PDF2 release 1999 and ICSD release 2004. Whole pattern fitting was done with TOPAS 4.2 software to determine the quantitative fractions of the crystalline phases.

The glass capillary samples were analyzed with the parallel beam setup in place. The scan parameters were: range 30-110° 2θ, step size 0.015° 2θ, and a hold time of 0.3 s/step. The capillary samples were spun during the scan collections to minimize crystal orientation effects.

The hot stage was evacuated to $\sim 1.3 \times 10^{-3}$ Pa for the duration of the experiments. Copper K_α radiation was used with a goniometer radius of 250mm, 0.3° fixed divergence slit, and a LynxEye PSD with an angular range of 3°. Scan parameters were: range 30-110° 2θ, step size 0.015° 2θ, and a hold time of 0.3 s/step.

In Table 2, we report the target base composition for the melts that have been made in this study. Additional melts were made containing 25, 50, and 100 mass% more Re than the base and the base plus 10 mass% ZrO₂.

4. Results

4.1 Metal Analyses

A portion of base composition (Pellet-5) was dissolved in HNO₃ and the solution sent for analysis with inductively-coupled plasma mass spectrometer (ICP-MS). The results from this analysis are shown in Table 2. While the analyzed and target compositions differ somewhat, there does not appear to be any significant loss of Pd from volatilization. No other samples were so analyzed, although we routinely obtained compositions from the EDS on the SEM. Additional samples need to be analyzed in this manner or with an electron microprobe.

Table 2. Target base composition for the ϵ -metal

Element	Composition	
	mol%	mass%
Mo	40.00	35.39
Pd	15.00	14.72
Re	10.00	17.17
Rh	5.00	4.75
Ru	30.00	27.96

4.2 X-Ray Diffraction

Two methods for obtaining X-ray diffraction patterns were used: the specimen was mounted in the spectrometer with a polished side in the beam. Because the specimens were cooled rapidly from below, the XRD pattern shows evidence of preferred orientation (Figure 1). This is evident in the peak at approximately 82° 2 θ . These metals are very hard and cannot be filed with a standard file. Therefore, a second method was developed in which the metal is first cooled to liquid N₂ temperature (77 K). The cold metal was quickly removed to a hammer mill. While cold, the metal exhibited some brittleness and, with repeated cycles of cooling and hammering, we obtained enough powder to obtain a good powder pattern. These patterns showed little or no preferred orientation.

Although the constituent metals have very different crystal structures (pure Mo is body-centered cubic; Re, Ru, and Tc hexagonal; Rh and Pd face-centered cubic), these alloys had the P6₃/mmc structure. The lattice parameters did not vary much from $a = 0.27611$ nm and $c = 0.44335$ nm. This appears to be common for these metals as the alloy MoPd_{0.3}Rh_{0.3}Ru_{0.4} has lattice parameters of 0.27650 nm and 0.44310 nm (PDF 00-051-0991) and ReTc (PDF 01-072-3068) has 0.27500 nm and 0.44370 nm, both with the P6₃/mmc crystal structure. This seems to indicate that this structure is flexible and can accommodate variations in composition, with minimal changes in the size of the unit cell.

A sample of this metal was placed in the high temperature stage of the XRD to determine the effect of increasing temperature on the crystal structure and if melting occurred at what temperature. Three runs were made. In the first run, the specimen was heated at 50°C/min and XRD patterns taken at each temperature. Because we did not know if the specimen would melt, we limited the first run to a maximum of 1000°C. In the second run, we heated the specimen rapidly to 1000°C then at

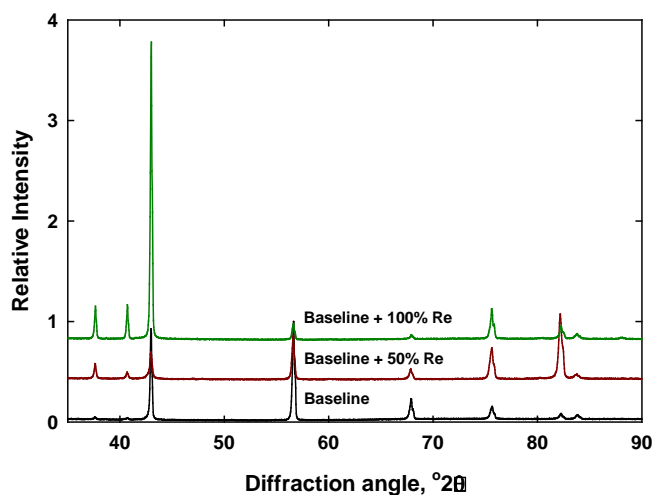


Figure 1. Set of XRD patterns from three ϵ -metal alloy specimens. Preferred orientation is evident from the intensity of the diffraction peak at approximately 82° 2 θ .

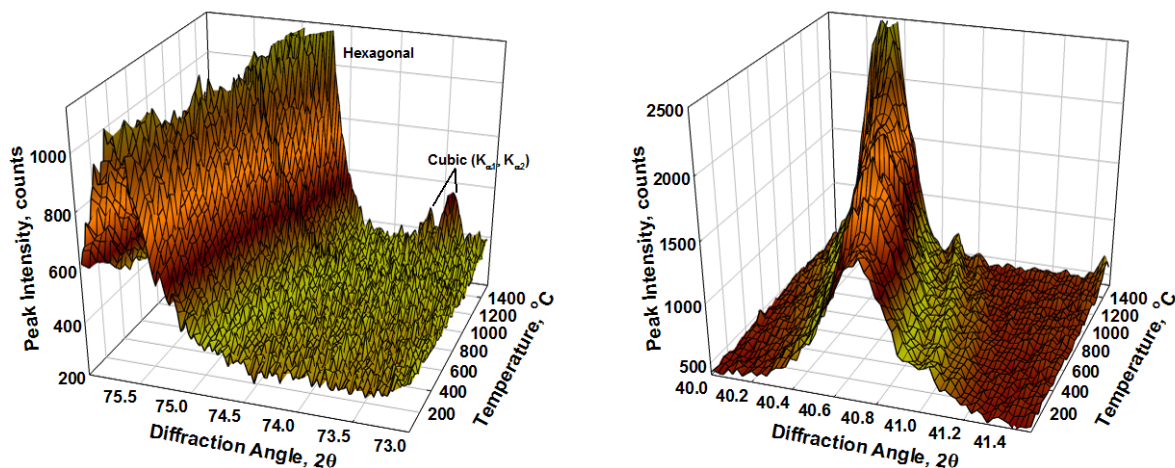


Figure 2. A summary of XRD patterns showing the effect of increasing temperature on the crystal structure of an ϵ -metal specimen with the base composition. The set of patterns on the left show more clearly the ingrowth of the cubic phase (Im3m); ingrowth is very subtle, occurring as a broadening of the peak on the high angle side. For clarity, the diffraction angles increase in opposite directions in these graphs.

50°C/min to 1500°C. No melting was observed. Finally we heated the specimen to 1550°C and held the temperature for 1.5 h to observe the in growth of a cubic phase. In Figure 2, the portions of the set of XRD patterns are shown to illustrate the ingrowth of the cubic phase. In the high angle graph, the ingrowth can be seen as two minor diffraction peaks that can only be indexed on a cubic lattice with $a = 0.28903$ nm. The change in the cubic unit cell dimension with temperature is small with $a = 0.28903$ nm at 1000°C and 0.28976 nm at 1500°C (Figure 3). There is much more variation in the hexagonal lattice parameters as seen in Figure 2 and Figure 3 with the expansion mainly in the c direction.

To more clearly illustrate the peak overlap between the most intense metal peaks for both the hexagonal and cubic phases, Figure 4 shows raw patterns at 1550°C after 1 hour and after quenching to 25°C. Also shown are the fitted peaks for each phase. After the specimen is quenched, the cubic phase remains; it is unclear if it would remain on slow cooling. The most intense peaks for each phase are: the (002) peak of the hexagonal phase and the (011) peak of the cubic phase. The presence of a cubic phase is not evident from the raw spectra, but becomes evident once the software fit is completed. However, the high-angle peak belonging to the cubic phase (211) is needed to make this assignment; it does not suffer from overlap with the closest hexagonal peak (013) and is a definitive confirmation of the cubic phase. The cubic (211) peak has weak intensity, ~13 % relative to (002), and thus has lower sensitivity than the (002) cubic peak.

With increasing time at 1500°C, the amount of cubic phase increases (Figure 5). Additional experiments are needed to determine if the rate is diffusion control and to determine the extent of cubic phase formation.

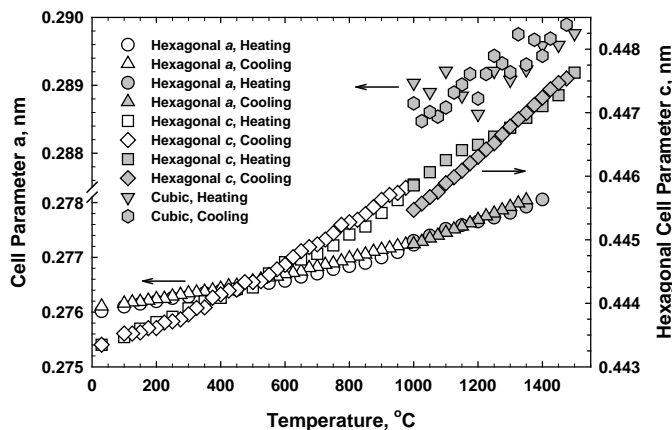


Figure 3. A graph showing the variation in lattice parameters with temperature for both the hexagonal and cubic phases. Part of the offset in data sets is from a lack of temperature calibration for the hot stage.

Table 3. Lattice parameters and unit cell volume changes with changes in Re content.

% Extra Re	<i>a</i> , nm	Uncertainty, nm	<i>c</i> , nm	Uncertainty, nm	Cell Volume, nm ³	Uncertainty, nm ³
0	0.27611	0.00003	0.44335	0.0000538	0.0292704	9.91×10 ⁻⁶
25	0.276149	0.0000264	0.44326	0.00005	0.0292727	8.90×10 ⁻⁶
50	0.275985	0.0000583	0.442985	0.0001077	0.0292198	1.95×10 ⁻⁵
100	0.276023	0.0000779	0.443503	0.0000786	0.0292621	2.17×10 ⁻⁵

Increasing the Re content of the metal causes no change in the lattice parameters or cell volume within the uncertainty of the determination (Table 3). This result is consistent with the data in the powder diffraction file for metals containing Mo, Pd, Re, Rh, Ru, or Tc.

Melting the metal with 10 mass% ZrO₂ made the material more difficult to melt, probably resulting in higher temperatures. The result was a metal with isolated pockets of baddeleyite (ZrO₂) that was partly sintered. The metal phase contained both hexagonal and cubic. The latter is probably the result of the high melting temperature and subsequent quenching. As indicated above, at temperatures above 1000°C, a cubic phase grows into the metal phase.

4.3 SEM Characterization

Specimens were cut from each main pellet with a diamond saw and polished with diamond paste. From the examination, it is clear that at least two phases are present (Figure 6). The basic difference between the two phases is the Mo, Pd, and Re contents (Table 4). From a cluster analysis, we have determined that there are approximately equal volumes of each of these phases.

In addition to the metal specimens, we also examined the metal melted with 10 mass% ZrO₂. The EDS results were inconclusive on the presence of the five metals in the ZrO₂. It appeared that some of the metal phase was present as a contaminant rather than as a result of reaction between the metal and the ZrO₂. There was no evidence of Zr in the metal phases.

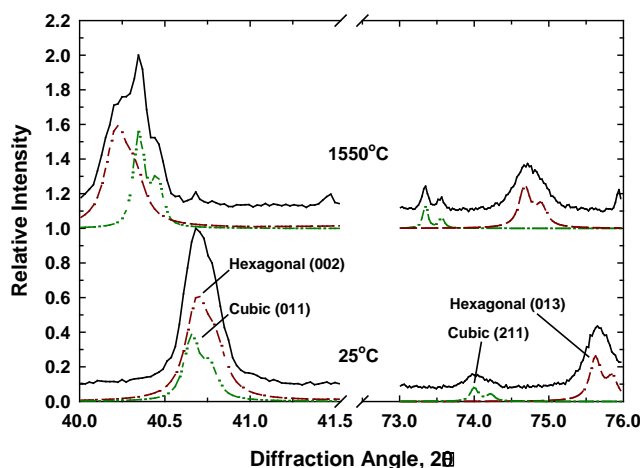


Figure 4. A comparison of the positions of two diffraction peaks from the metal phase heated to 1550°C and quenched. The lone diffraction peak at approximately 74° 2θ allowed us to determine the presence of a cubic phase; it could not be established from the high intensity peak at approximately 40.7° 2θ.

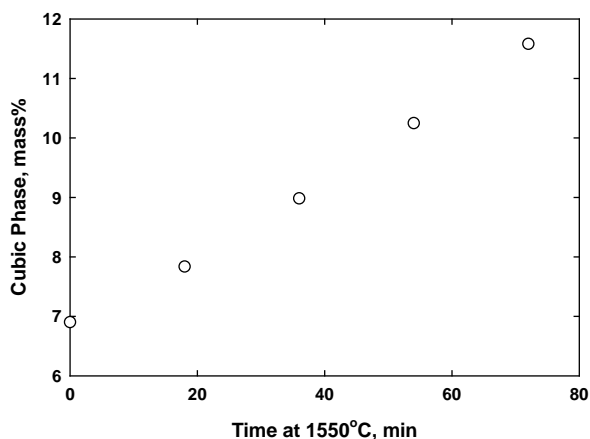


Figure 5. A graph showing the variation in the amount of cubic phase with increasing time at 1550°C.

Table 4. The typical compositions of the two phases found in the ϵ -metal, where the element in the second column indicates the enriched metal.

Specimen Enrichment in Re	Phase	Mo	Ru	Rh	Pd	Re
25	Pd	41.0	30.3	3.4	16.6	8.8
25	Re	38.9	33.8	3.7	11.1	12.6
50	Pd	40.8	29.7	3.2	15.7	10.5
50	Re	36.9	33.4	3.5	9.2	17.0

4.4 TEM Characterization

The structure was confirmed through examination of selected area electron diffraction (SAED) patterns at several zone axes. In Figure 7, an electron diffraction obtained along $\mathbf{B}[121]$ is shown together with a simulated diffraction pattern. The molecular model shows the structure projected along a random direction. All SAED results were compared to simulated diffraction patterns generated with CrystalMaker™ software. Although the phase is hexagonal, the indices are listed as Miller indices which can be converted to Miller-Bravais indices by standard methods. The measured angle between (111) and (101) was 101° ; whereas the calculated value for *hcp*-Ru is 103.1° . The convergent beam electron diffraction (CBED) method may be the most precise method for looking for structural differences between the Re- and Mo-rich regions. Areas outlined by higher order Laue zone (HOLZ) lines could be used for comparison; the indexing of the HOLZ lines provides a direct method for determining unit cell parameters or the c/a .

The material was wedged-shaped with steeply angled faces that made diffraction patterns or images difficult to obtain. Although in general, the material was defect free, some defects were found (Figure 8). There were few signs of any gross microstructure including grain boundaries. Compositional variations in the metal were found (Figure 6), but these could not be seen readily in the TEM images. The specimen was analyzed with EDS and the Mo/Re signal was monitored (Figure 9). As the composition suggested a change, the sample was observed again on the diffraction plane. Surprisingly, there was little or no change in the crystallographic orientation. This indicated that not only did the Mo-rich and Re-rich zones possess the same structure, but that neighboring regions had the same orientation. This would suggest that the phases formed through an exsolution process that allowed the separation of Mo and Re, but preserved the overall structure, including the crystal orientation. The CBED patterns (Figure 9) show a slight change in angle primarily from bends in the specimen foil but the overall orientation was identical. The CBED technique can be extremely accurate for measuring unit cell parameters; hence an effort was made to elucidate the structure with CBED. Figure 10, shows the first attempt at doing this. A CBED pattern

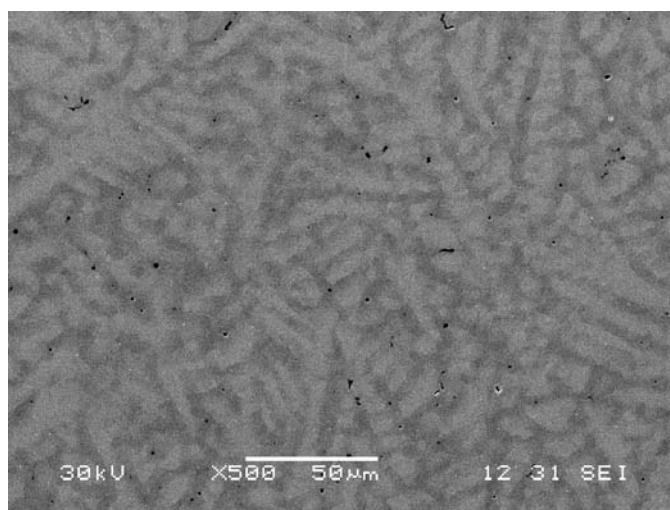


Figure 6. A backscattered electron photomicrograph of the typical microstructure in the ϵ -metal, in this case the base composition plus 25 mass% Re.

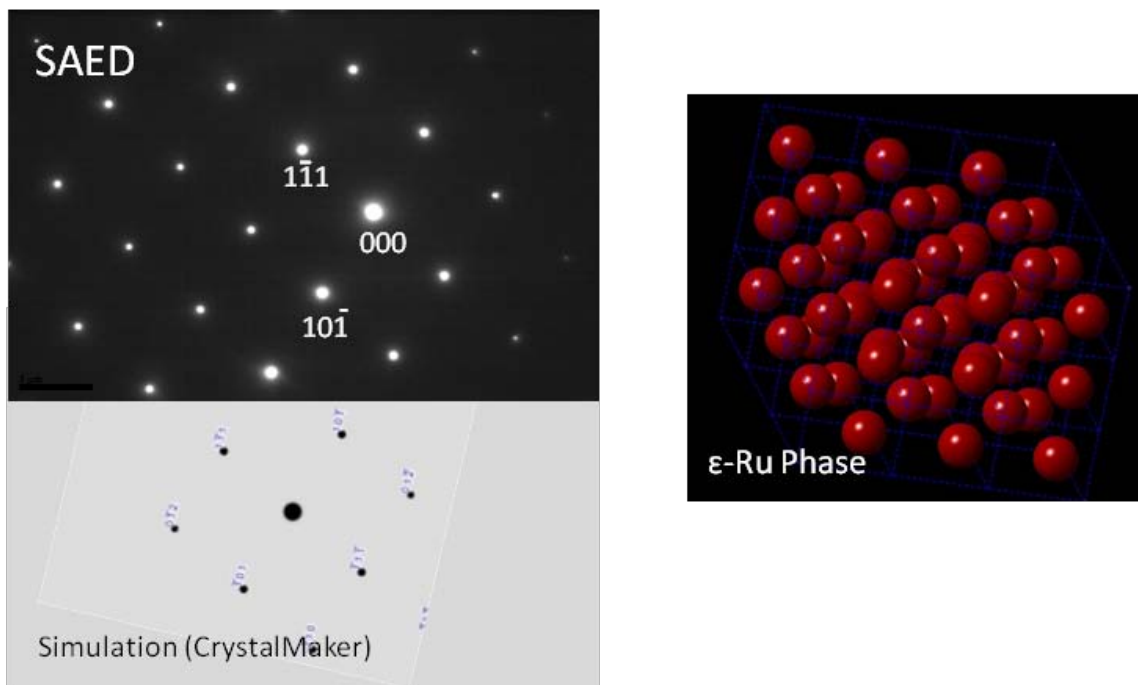


Figure 7. Electron diffraction pattern taken along the B[121] zone axis, with computer simulation of the diffraction pattern and a molecular model generated from the structural data for hexagonal ruthenium metal.

was recorded near a known zone axis and the fine lines (HOLZ) were measured and indexed with the computer simulations. The angles between planes and distances between lines will be useful measures for determining small structural changes in the unit cell parameters.

Figure 8 Images showing grown-in defects in metal taken along (a) $g = 002$ and (b) $g = 100$.

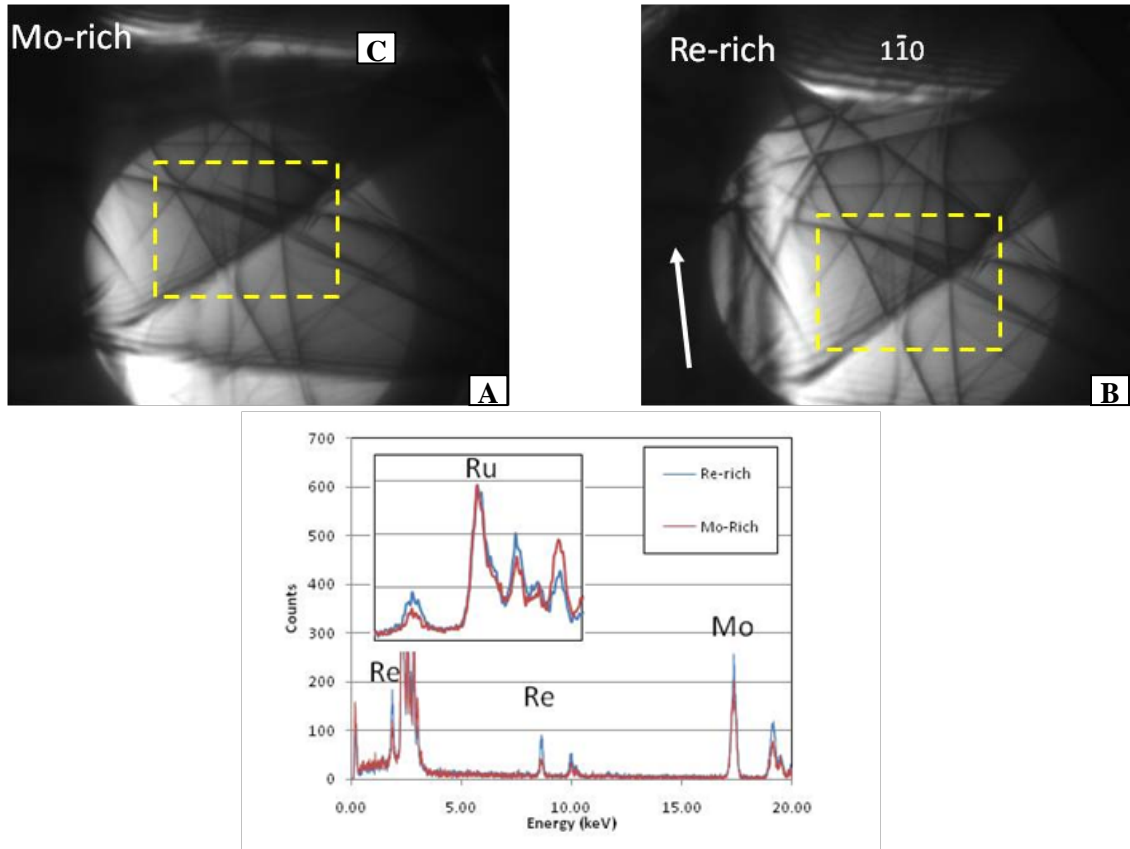


Figure 9. Convergent beam electron diffraction patterns taken with $g=110$ between compositionally different areas. The yellow box outlines a region that is common to both patterns. Also shown are the results of the EDS analyses of the regions of interest. The insert shows the slight difference in composition.

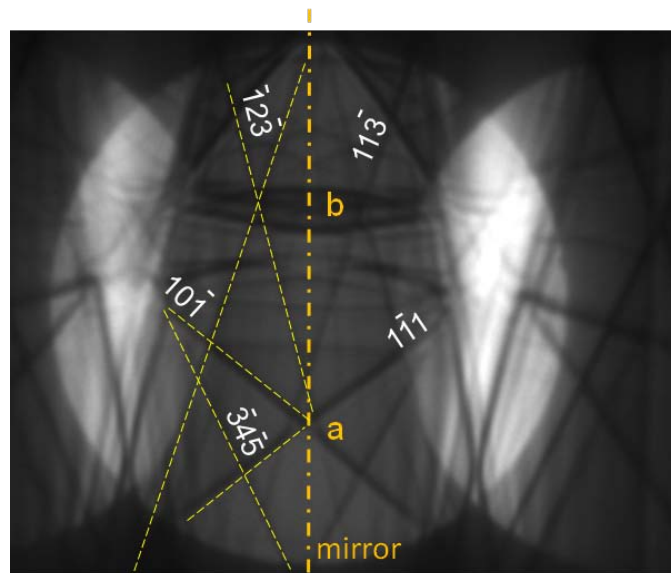


Figure 10. A CBED pattern close to B[121] with some higher order Laue zones indexed.

5. Conclusions

There are two apparent reasons for selecting the ϵ -metal phase for use as a waste form. It is found in the undissolved solids from the dissolution of nuclear fuel in strong acid. Remnants of this phase are found in the natural reactors at Gabon, Africa where the environmental conditions were very harsh – much more so than would be expected in a repository, except under the conditions of magma intrusion. The metal waste form would be formed by arc melting the ϵ -metal particles into an ingot without any dilution from other metals.

Results to date indicate that the combination of Mo, Pd, Re (a stand-in for Tc), Rh, and Ru yields a metal with nearly invariant unit cell parameters with composition. The metal samples made to date consist of a single phase, but one in which there are high Re and high Pd regions. The XRD pattern can only be indexed to a single phase with the hexagonal close packing structure with the space group $P6_3/mmc$. These results are similar to those found by Kleykamp and coworkers (1985) for the metal phases with the hexagonal structure found in irradiated fuel.

We also melted metal with 10 mass% ZrO_2 as a stand-in for the other oxygen-bearing phases present in the UDS. These results indicate that the ZrO_2 was unreacted and remained in the metal as isolated pockets as the mineral baddeleyite. No evidence for Zr dissolved into the metal phase was found. A cubic phase was found that was consistent with the high-temperature XRD results that indicate the ingrowth of a cubic phase above $1000^\circ C$. The presence of the cubic phase in this melt is probably the result of the higher temperatures required to melt this material and the rapid quenching of the sample.

The results of the studies done to date suggest that the ϵ -metal is a robust waste form that is flexible with respect to composition. Melting of the metal can be done with a non-volatile oxide, such as ZrO_2 , as a stand-in for oxide phases in UDS. This oxide is immobilized in the metal matrix as isolated pockets. Studies of the UDS have not resulted yet in a clear definition of its composition. Kleykamp and coworkers (1985), for example, found that one of the compounds present in the UDS was $(Ba_{1-x-y}Sr_xCs_y)(U, Pu, RE, Zr, Mo)O_3$ [RE = rare earth element]. Additional studies are needed with more realistic UDS and stand-in materials.

6. Future Work

The electrochemical corrosion characterization of these metals is needed to compare against previous work (Cui, Eriksen and Eklund 2001). We will examine these materials with an electrochemical atomic force microscope that will allow us to examine each phase in situ. The information on the parts of the material with different composition will complement the standard electrochemical tests that will be performed on the metal waste form being developed at Argonne National Laboratory and will also be performed on the ϵ -metal waste form. Additional work will be done to refine the process by which this metal is made and made with UDS present. Studies are underway at other laboratories to define the UDS and we will use this information when it is available. The dissolution rate of ϵ -metal and metal plus UDS needs to be investigated both with electrochemical and single-pass flow-through tests. Finally, we will also investigate methods for recovery of Tc, Mo, and the platinum metals from the other parts of the recycle process so that they can be incorporated into the ϵ -metal phase.

7. References

Cui, D, T Eriksen, and U-B Eklund. 2001, "On Metal Aggregates in Spent Fuel, Synthesis and Leaching of Mo-Ru-Pd-Rh Alloy." *Materials Research Society Symposium Proceedings* 663:427-34.

Gauthier-Lafaye, F, P Holliger, and PL Blanc. 1996, "Natural Fission Reactors in the Franceville Basin, Gabon: A Review of the Conditions and Results of a "Critical Event" in a Geologic System." *Geochimica et Cosmochimica Acta* 60:4831-52.

Gombert II, D. 2007, Global Nuclear Energy Partnership Integrated Waste Management Strategy Waste Treatment Baseline Study, Volume I. Technical Rpt. GNEP-WAST-AI-RT-2007-000324, Idaho National Laboratory, Idaho Falls, ID.

Hidaka, H, and P Holliger. 1998, "Geochemical and Neutronic Characteristics of the Natural Fossil Fission Reactors at Oklo and Bangombé, Gabon." *Geochimica et Cosmochimica Acta* 62:89-108.

Kleykamp, H. 1985, "The Chemical-State for the Fission-Products in Oxide Fuels." *Journal of Nuclear Materials* 131:221-46.

Kleykamp, H. 1988, "The Chemical-State of the Fission-Products in Oxide Fuels at Different Stages of the Nuclear-Fuel Cycle." *Nuclear Technology* 80:412-22.

Kleykamp, H. 1987, "Composition after Dissolution in HNO₃ of the Residue of Knk-II-I Fuel." *Atomwirtschaft-Atomtechnik* 32:235-36.

Kleykamp, H, JO Paschoal, R Pejsa, and F Thummler. 1985, "Composition and Structure of Fission-Product Precipitates in Irradiated Oxide Fuels - Correlation with Phase Studies in the Mo-Ru-Rh-Pd and Ba-UO₂-ZrO₂-MoO₂ Systems." *Journal of Nuclear Materials* 130:426-33.

Kleykamp, H, and R Pejsa. 1984, "X-Ray Diffraction Studies on Irradiated Nuclear-Fuels." *Journal of Nuclear Materials* 124:56-63.

Utsunomiya, S, and RC Ewing. 2006, "The Fate of the Epsilon Phase (Mo-Ru-Pd-Tc-Rh) in the UO₂ of the Oklo Natural Fission Reactors." *Radiochimica Acta* 94:749-53.

Wronkiewicz, DJ, CS Watkins, AC Baughman, FS Miller, and SF Wolf. 2002, "Corrosion Testing of Simulated Five-Metal Epsilon Particle in Spent Nuclear Fuel." *Materials Research Society Symposium Proceedings* 713:625-32.